ARTICLES
PUBLISHED ONLINE: 27 FEBRUARY 2011 | DOI: 10.1038/NPHYS1928
nature physics

Time-resolved measurement of spin-transfer-driven ferromagnetic resonance and spin torque in magnetic tunnel junctions

Chen Wang[1], Yong-Tao Cui[1], Jordan A. Katine[2], Robert A. Buhrman[1] and Daniel C. Ralph[1,3]*

The bias dependence of the torque that a spin-polarized current exerts on ferromagnetic elements is important for understanding fundamental spin physics in magnetic devices and for applications. Several experimental techniques have been introduced in recent years in attempts to measure spin-transfer torque in magnetic tunnel junctions. However, these techniques have provided only indirect measures of the torque and their results regarding bias dependence are qualitatively and quantitatively inconsistent. Here we demonstrate that spin torque in magnetic tunnel junctions can be measured directly by using time-domain techniques to detect resonant magnetic precession in response to an oscillating spin torque. The technique is accurate in the high-bias regime relevant for applications, and because it detects directly small-angle linear-response magnetic dynamics caused by spin torque it is relatively immune to artefacts affecting competing techniques. At high bias we find that the spin-torque vector differs markedly from the simple lowest-order Taylor series approximations commonly assumed.

Spin-transfer torque allows the magnetization in magnetic devices to be manipulated efficiently using the interaction of spin-polarized currents with ferromagnets[1–3]. The behaviour of spin torque for high biases (V) applied to magnetic tunnel junctions (MTJs) provides a sensitive probe into the fundamental spin physics of hot electrons and is critical for applications, including next-generation memory devices and tunable oscillators[4]. However, measurements of spin torque in this regime have proven difficult. Previous approaches, based on different indirect measures of the torque, have yielded conflicting results[5–17]. Here we demonstrate an improved method of measuring spin torque by detecting, in a time-resolved fashion, the magnetic dynamics in linear response to the torque. Because this technique measures directly the small-angle precession caused by the torque, it is much less vulnerable than previous techniques to artefacts arising from heating or nonuniform magnetic dynamics. The method allows quantitative measurements of the bias dependence of the spin-torque vector at large $|V|$, up to the breakdown voltage of the MTJ, and reveals behaviour strikingly different from the approximations normally used to interpret experiments.

Several different approaches have been used previously in efforts to measure spin torque in MTJs. For measurements at low-to-moderate $|V|$, we believe that the most accurate technique is spin-transfer-driven ferromagnetic resonance (ST-FMR) with detection of magnetic precession via a d.c. mixing voltage[5–9]. However, this method fails at large $|V|$ because of an artefact associated with small changes in the d.c. resistance of MTJs in response to a microwave drive[9]. Analysis of the statistics of thermally assisted switching can be used to extract the spin torque at large $|V|$ (refs 10,11), but this method requires assuming a particular functional form for the bias dependence of the torque, it is sensitive to assumptions made about heating, and different analyses have yielded qualitatively different behaviours for the perpendicular, or 'field-like', component of the spin-torque vector[10,11]. Thermally excited ferromagnetic resonance (TE-FMR; refs 13–17) is another technique that can in principle measure the perpendicular spin-torque component, based on the bias dependence of the precession frequency, but the results of this method can be questioned[9] because a bias may also affect the precession frequency via other mechanisms, including Joule[13] or Peltier heating or changes in the degree of spatially nonuniform dynamics due to lateral spin diffusion[18,19].

Measurement scheme

The concept of our technique is to apply a microwave current through the MTJ to exert an oscillating spin-transfer torque near the magnetic resonance frequency of one magnetic electrode, and to measure the resulting magnetic precession via oscillations of the MTJ resistance. Our measurement circuit is illustrated in Fig. 1a. To accomplish the measurement, we apply two electrical pulses simultaneously to the MTJ via a 50 Ω transmission line: a microwave (RF) pulse $V_{\rm in}(t)$ with length 5–10 ns, long enough to reach steady-state resonant magnetic precession via the spin-torque effect, together with a longer square-wave pulse (∼25 ns length) that starts a few nanoseconds earlier and ends several nanoseconds later than the RF pulse so that it provides the equivalent of a d.c. bias during the resonance measurement. We record the signal reflected from the sample using a 12.5 GHz bandwidth sampling oscilloscope. The time-dependent part of the reflected voltage (before amplification) is:

$$V_{\rm ref}(t) = \frac{(50\,\Omega)}{R_0 + (50\,\Omega)} I\,\Delta R(t) + \frac{R_0 - (50\,\Omega)}{R_0 + (50\,\Omega)} V_{\rm in}(t)$$

The first term on the right is the signal from the resistance oscillation that we aim to measure, with I the effective d.c. current through the device provided by the square-wave pulse and $\Delta R(t)$ the time-dependent part of the MTJ resistance. The second term arises from the reflection of $V_{\rm in}(t)$ from the impedance discontinuity between the 50 Ω cable and the sample with differential resistance

[1]Cornell University, Ithaca, New York 14853, USA, [2]Hitachi Global Storage Technologies, San Jose Res. Ctr., San Jose, California 95135, USA, [3]Kavli Institute at Cornell, Cornell University, Ithaca, New York 14853, USA. *e-mail: ralph@ccmr.cornell.edu.

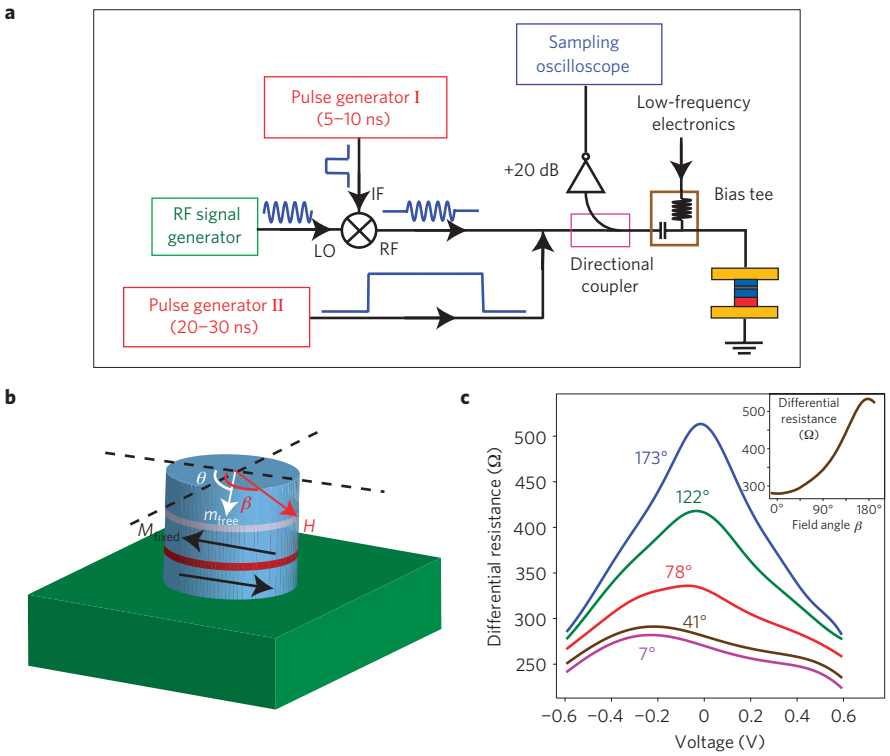

Figure 1 | Overview of the experiment. a, Schematic of our measurement circuit. **b**, Geometry of the MTJ devices. **c**, (Main panel) Bias dependence of the differential resistance for sample 1 at selected offset angles θ as labelled, (inset) zero-bias resistance as a function of field angle β for $H = 600$ Oe.

R_0. One might consider trying to determine $\Delta R(t)$ by simply measuring the reflected signal during the time when $V_{in}(t)$ is nonzero, but the term due to the impedance discontinuity is generally 1–2 orders of magnitude larger than the term involving $\Delta R(t)$, and it is difficult to subtract this large background. Instead, we achieve a better signal-to-noise ratio by recording the reflected signal shortly (100 ps–2 ns) after the falling edge of the RF pulse. In this time span, the resistance oscillation excited by the RF pulse (ST-FMR) is still present (although gradually decaying) whereas the strong background due to $V_{in}(t)$ is diminished. After subtracting the much weakened background, we are able to clearly resolve the resistance oscillation of the MTJ. The details of the measurement are explained in the Methods section and Supplementary Note S1. A discussion about why the technique is relatively immune to artefacts from heating and spatially nonuniform magnetic dynamics is given in Supplementary Note S2.

Sample geometry

We have measured MTJs with the following layer structure (in nanometres): bottom electrode [Ta(3)/CuN(41.8)/Ta(3)/CuN (41.8)/Ta(3)/Ru(3.1)], synthetic antiferromagnet (SAF) layer pinned to IrMn [IrMn(6.1)/CoFe(1.8)/Ru/CoFeB(2.0)], tunnel barrier [MgO_x], free layer [CoFe(0.5)/CoFeB(3.4)] and capping layer [Ru(6)/Ta(3)/Ru(4)]. Both the free layer and the SAF pinned layer are etched into a circular shape with nominal diameter either 80 or 90 nm. The devices have a nominal resistance–area (RA) product of 1.5 $\Omega\,\mu m^2$ and measured tunnel magnetoresistance (TMR) ratios of 85–100%. We monitor the resistance and TMR throughout the experiment to ensure that the MTJs are not degraded at high bias[20]. The capacitance is $<5 \times 10^{-14}$ F, small enough that it does not affect the experiment (see Methods). During the measurements, we apply an in-plane magnetic field H (200–450 Oe) at an angle β (45°–135°) relative to the exchange bias of the SAF to produce a nonzero offset angle θ between the free layer and the reference layer of the SAF (Fig. 1b). We use the convention that positive bias corresponds to electron flow from the free layer to the SAF (so that the in-plane spin torque favours antiparallel alignment). We have measured ten samples, all with similar results, and we will report data from two of them. Sample 1 (nominally 90×90 nm^2) has a parallel-state resistance of 272 Ω and TMR of 91% (Fig. 1c), and sample 2 (nominally 80×80 nm^2) has a parallel-state resistance of 381 Ω and TMR of 97%.

ST-FMR in the time domain

Each time-domain measurement is performed in two steps. For each value of H for which a measurement is desired, we measure the differential resistance of the MTJ and also identify a different set of biasing conditions (field magnitude and direction) with the same value of differential resistance but which is non-resonant, in the sense that the magnetic resonance condition is well outside the frequency range of interest. We measure the RF pulse reflected from the sample under the non-resonant conditions to determine the background signal in the absence of magnetic dynamics. Figure 2a shows a typical background signal near the falling edge of the RF pulse (vertical dashed line). We then measure the signal reflected from the sample for the biasing conditions that are of interest for measuring the magnetic dynamics, and subtract the background (Supplementary Note S1 and Fig. S1). Figure 2b,c show the result of this subtraction for the case of $H = 200$ Oe, field direction $\beta = 90°$, offset angle $\theta = 85°$, $V = 0.38$ V for sample 1. Following the falling edge of the RF pulse, the measurement shows a resistance oscillation that decays gradually in time. The magnitude of oscillation corresponds to a maximum precession angle of about 1.5°, well within the linear-response regime. The decay rate for the oscillations agrees quantitatively with the magnetic damping rate measured by d.c.-detected ST-FMR in the same samples (Supplementary Note S4 and Fig. S2), indicating that the decay is due to a true decrease in precession amplitude, and is not dominated by dephasing between different repetitions of the measurement. Ideally our background subtraction should work not only after the

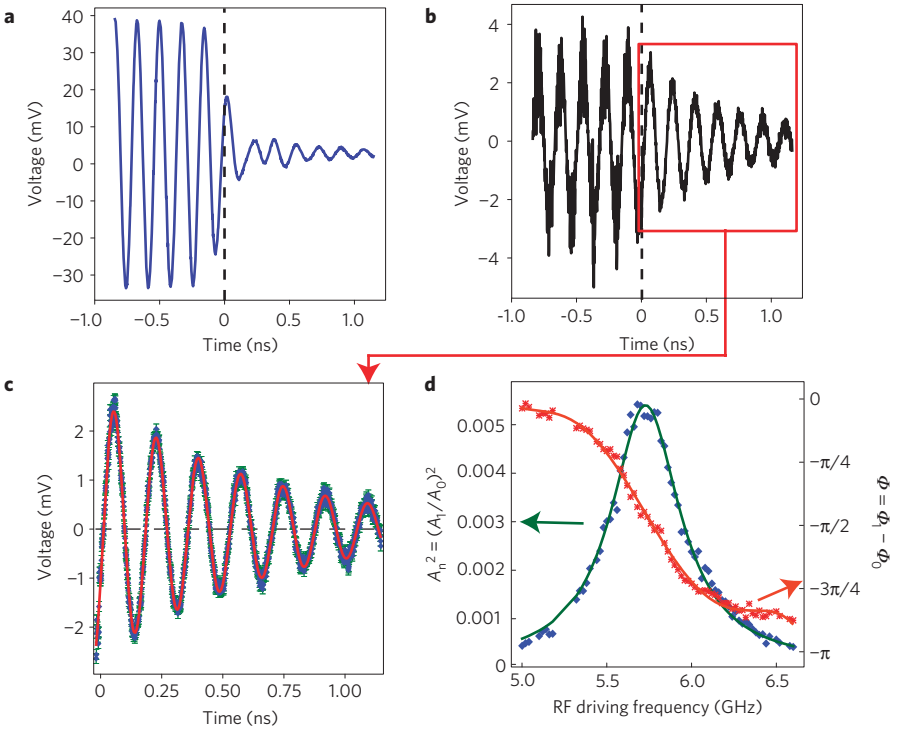

Figure 2 | Time-resolved measurements of spin-torque-driven magnetic resonance. a, Falling edge of the applied waveform (for a 5.8 GHz RF pulse), measured on reflection from sample 1 with the MTJ biased at a non-resonant state with magnetic field $H = 600$ Oe (field direction $\beta = 94°$) and voltage $V = 0.38$ V. This waveform represents the background in the resonance measurement. **b**, The reflected voltage waveform from sample 1 near magnetic resonance after background subtraction for an applied magnetic field $H = 200$ Oe, field direction $\beta = 90°$, offset angle $\theta = 85°$, $V = 0.38$ V. This signal is proportional to the resistance oscillations of the MTJ excited by the resonant RF pulse shown in **a**. **c**, Close-up view of the measured oscillations in **b** from the time span after the falling edge of the RF pulse, along with a fit to a decaying sinusoidal curve (red line). **d**, Dependence on the frequency of the RF drive pulse (for the same biasing conditions as in **b**) for the normalized oscillation amplitude squared $A_n^2 = (A_1/A_0)^2$ (diamonds) and the oscillation phase relative to the drive pulse, $\Phi = \Phi_1 - \Phi_2$ (asterisks). The green curve is a symmetric Lorentzian fit to the amplitude data, and the red curve is a smooth polynomial fit of the phase.

RF pulse but also during the pulse, and we have indeed resolved the steady-state persistent resistance oscillation during the pulse as well (for time <0 in Fig. 2b). This persistent oscillation confirms that the RF pulse is long enough to saturate the MTJ to steady-state dynamics. However, the oscillations measured during the pulse are noisy because of the large background that is subtracted, so we do not use them for quantitative analysis.

We fit the damped resistance oscillation following the falling edge of the RF pulse (Fig. 2c) to an exponentially decaying sinusoid $A_1 e^{-\Gamma t}\cos(\omega t + \Phi_1)$ with four parameters: amplitude A_1, phase Φ_1, frequency ω and decay rate Γ, defining the centre of the falling edge of the pulse as time zero ($t = 0$). The fitting uncertainty for the phase is less than 0.04 rad, which corresponds to a time precision of $\sim$1 ps. Using the same $t = 0$ point, we also fit the RF driving signal (Fig. 2a) before the falling edge of the pulse to a simple sinusoid $A_0\cos(\omega_0 t + \Phi_0)$ with fitting parameters A_0 and Φ_0. The phase of the magnetic response relative to the externally applied RF driving voltage is then $\Phi = \Phi_1 - \Phi_0$. In Fig. 2d we plot the normalized oscillation amplitude squared, $A_n^2 = (A_1/A_0)^2$, and relative phase, Φ, as a function of the RF pulse frequency for the same biasing conditions shown in the other panels of Fig. 2. As expected (see the Supplementary Note S3), the resonant response is accurately fit by a symmetric Lorentzian line shape and the phase changes by π as the frequency is tuned through the resonance. We determine the natural frequency of the oscillator ω_m and the maximum normalized oscillation amplitude $A_{n,max}$ from the fit to the amplitude response, and then determine the phase Φ_m of the magnetization precession at resonance by interpolating to the value at ω_m on a smooth polynomial fit of Φ versus driving frequency.

Determination of the spin-transfer torque

From the values of $A_{n,max}$, Φ_m, and Γ we make a quantitative determination of the spin-torque vector. Because it is a torque, this vector is perpendicular to the mean magnetization of the free layer and therefore we can specify it using two components, one in the plane determined by the magnetizations of the two electrodes ($\tau_\parallel$) and one perpendicular to this plane ($\tau_\perp$). A consideration of the equation of motion for the free layer magnetization shows that an oscillating in-plane torque on resonance gives rise to a resistance oscillation in phase with the driving voltage ($\Phi_m = 0$), whereas an oscillating perpendicular component independently contributes an out-of-phase resistance oscillation. Quantitatively, it follows that the voltage derivative of the torque, or 'torkance'[21] $\partial\boldsymbol{\tau}/\partial V$, can be calculated from the in-phase and out-of-phase magnetic response at any bias V (see Supplementary Note S3 for the derivation):

$$\left.\frac{\partial \tau_\parallel}{\partial V}\right|_\theta = \cos\Phi_m \frac{[R_0 - (50\,\Omega)][(R_0 + 50\,\Omega)]}{R_0(50\,\Omega)} \times \frac{\hbar}{2}\frac{M_S \mathrm{Vol}}{\mu_B I}\left(\left.\frac{\partial R}{\partial \theta}\right|_I\right)^{-1} \Gamma A_{m,max} \quad (1)$$

$$\left.\frac{\partial \tau_\perp}{\partial V}\right|_\theta = -\sin\Phi_m \frac{[R_0 - (50\,\Omega)][(R_0 + 50\,\Omega)]}{R_0(50\,\Omega)} \times \frac{\hbar}{2}\frac{M_S \mathrm{Vol}}{\mu_B I}\left(\left.\frac{\partial R}{\partial \theta}\right|_I\right)^{-1} \frac{\Gamma A_{m,max}}{\Omega_\perp} \quad (2)$$

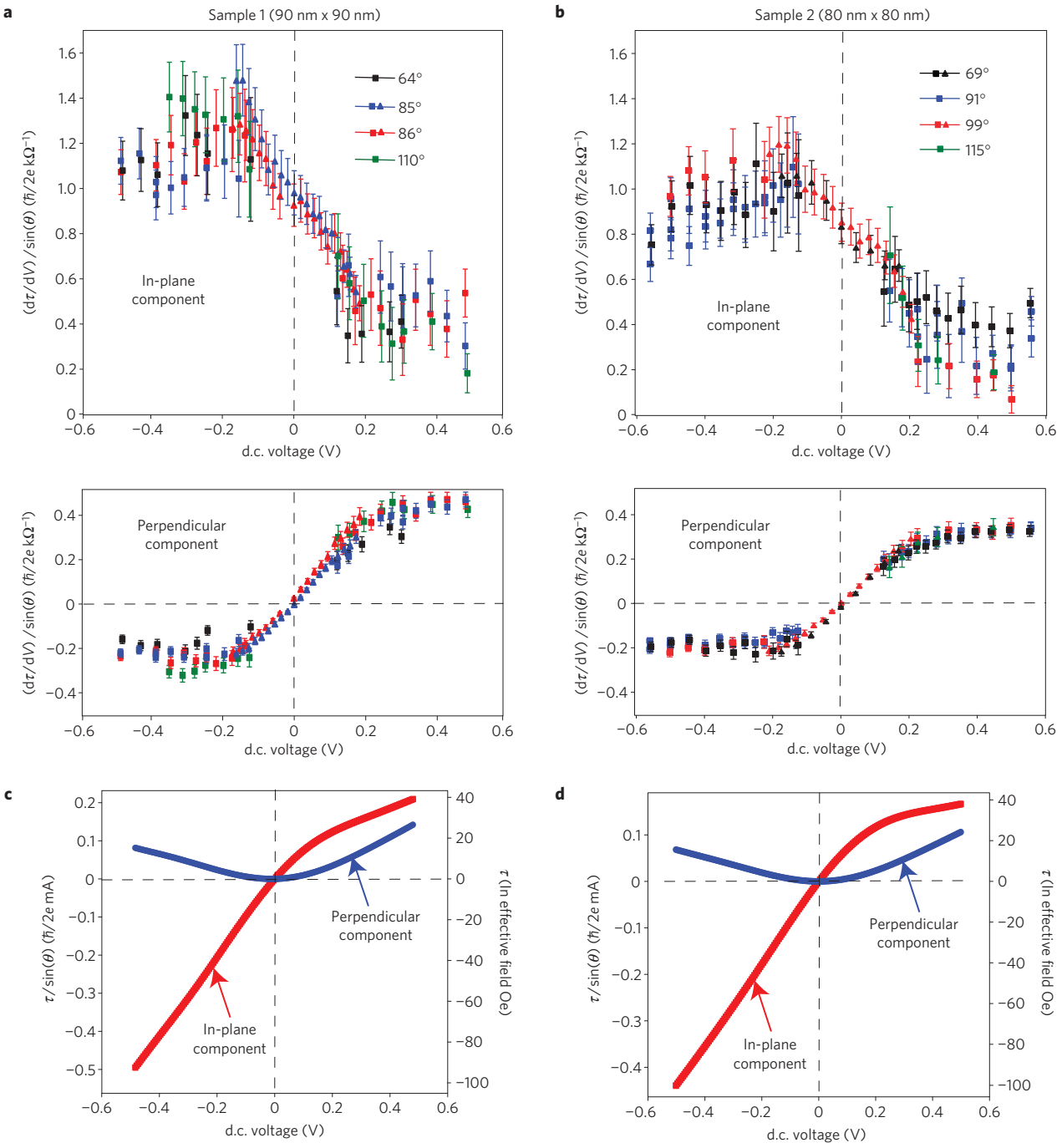

Figure 3 | Measured bias dependence of the spin-transfer torque vector. a,**b**, In-plane and perpendicular components of the torkance vector $\partial\boldsymbol{\tau}/\partial V$ (normalized by sin θ) as a function of bias voltage for sample 1 (**a**) and sample 2 (**b**), for different initial offset angles, θ. The square symbols correspond to our time-resolved measurements and the triangles to d.c.-detected ST-FMR on the same samples. Error bars for the results of the time-resolved measurements are derived from equations (1) and (2), taking into account one-standard-deviation fitting uncertainties for the oscillation amplitude $A_{m,max}$ and phase Φ_m and estimated uncertainties due to non-ideal pulse shapes and capacitance. Error bars in the d.c.-detected ST-FMR data are from ref. 9. **c**,**d**, In-plane and perpendicular components of the spin-transfer torque $\boldsymbol{\tau}$ (normalized by sinθ) for sample 1 (**c**) and sample 2 (**d**), determined by integrating the data in **a**,**b** after averaging over the different initial offset angles.

Here R_0 is the measured differential resistance of the MTJ for the initial offset angle θ and bias V, M_SVol is the total magnetic moment of the free layer (estimated to be 1.8×10^{-14} e.m.u.($\pm$15%) for our $90 \times 90\,nm^2$ devices and 1.6×10^{-14} e.m.u.($\pm$15%) for our $80 \times 80\,nm^2$ devices on the basis of vibrating sample magnetometer measurements of test films), μ_B is the Bohr magneton, $\partial R/\partial\theta|_I$ is the angular derivative of the d.c. resistance ($R = V/I$) of the MTJ, and $\Omega_\perp \approx 4\pi M_{eff}\gamma/\omega_m$ is a dimensionless factor (typically $\sim$5 in our experiment), where $4\pi M_{eff} = 13 \pm 1$ kOe is the easy plane anisotropy strength of the free layer film (estimated by comparing our measured ST-FMR frequency to a Kittel formula[22]). For the data of Fig. 2, this analysis yields $\partial\tau_\parallel/\partial V = (0.44 \pm 0.10)(\hbar/2e)\,k\Omega^{-1}$, $\partial\tau_\perp/\partial V = (0.47 \pm 0.03)(\hbar/2e)\,k\Omega^{-1}$ at $V = 0.38$ V. The dominant experimental uncertainties are associated with determining the oscillation phase. By varying the amplitude of the square-wave pulse (and therefore d.c. bias), we can

measure the spin-transfer torkance for any value of $|V|$ above about 0.1 V for our samples.

It should be noted that in response to a microwave excitation there is often more than one resonance mode in our devices at a given external field, usually one large amplitude mode and a second mode at least a factor of three smaller in amplitude. We suspect that the smaller mode involves oscillation of the magnetizations in the SAF, and that there may be coupling to the free layer oscillations. To limit the effects of mode coupling, for the data in this paper we have selected the direction and magnitude of the external magnetic field so that any secondary resonance mode is weak and well-separated in frequency from the primary resonance. The primary resonance can be identified with oscillations of the free magnetic layer on the basis of the sign of the resonant response in the d.c.-detected ST-FMR spectrum[6] and the sign of the bias dependence of the magnetic damping (see Supplementary Note S4 and Fig. S2).

Bias dependence of the spin torque

Figure 3a,b show our measurements of $\partial\tau_{\parallel}/\partial V$ and $\partial\tau_{\perp}/\partial V$ over a large bias range for two samples. We display data up to $|V| = 0.6$ V, because the distribution of critical voltages for sample degradation or breakdown in our low-*RA* MTJs extends below 0.7 V. We have normalized the torkances by $\sin\theta$, because this is the angular dependence predicted for MTJs (refs 21,23), and indeed we find good agreement with this dependence within our experimental uncertainty. The figures show both the results of our new time-domain measurements for $|V| > 0.1$ V (square symbols), and the results in the same samples of the older d.c.-detected ST-FMR technique[7,9] for $|V| < 0.2$ V (triangles), which is a sufficiently small bias that this technique is reliable. In the range of overlap, $0.1\,\text{V} < |V| < 0.2\,\text{V}$, we find excellent quantitative agreement between these two independent techniques with no adjustment of parameters. This cross-check provides added confidence that both methods are quantitatively correct. By integrating the torkances with respect to voltage, we can plot the bias dependence of the spin-torque vector $\boldsymbol{\tau}(V)$ itself (Fig. 3c,d).

We observe that the in-plane component of the spin-transfer torkance has an appreciable negative slope in the bias range $|V| < 0.2$ V in all of our MgO-based tunnel junctions, and is a factor of 3–4 stronger at high negative bias ($V < -0.2$ V) than at high positive bias ($V > 0.2$ V). Although this is a weaker bias dependence than had been suggested (incorrectly) in the past by uncorrected d.c.-detected ST-FMR measurements[8,9], the in-plane component of the spin torque after integration does show significant nonlinearity and can become stronger by approximately a factor of 2.5 at large negative bias compared to positive bias (Fig. 3c,d). Although an asymmetric bias dependence of the in-plane torkance is consistent with qualitative predictions[24–27] and *ab initio* calculations at low bias,[28] we suggest that a more quantitative theoretical understanding of the asymmetry at high bias should be a priority. Regarding the perpendicular component of the torkance, it had been known previously from calculations[24] and d.c.-detected ST-FMR measurements[7,8] that near $V = 0$ this component of the torkance in a symmetric MTJ has a linear dependence on bias (so that the perpendicular torque $\propto V^2$). We now observe departures from this behaviour at high bias, in that $\partial\tau_{\perp}(V)/\partial V$ saturates (and $\tau_{\perp}(V)$ crosses over to an approximately linear dependence). Interestingly, the saturated value of perpendicular torkance differs significantly between positive and negative bias, which is forbidden by symmetry for an exactly symmetric MTJ when spin-flip scattering is negligible[3]. We suspect that this may be the result of a slight asymmetry in the structure of our MTJs (for example, the average Co:Fe ratio in the reference layer of the SAF is 1.5:1, whereas in the free layer it is 1.25:1) or in the distribution of defects in the tunnel barrier or at the interfaces between the electrodes and the barrier. The strength of the perpendicular torque at the highest biases we measure is equivalent to a 30 Oe magnetic field, strong enough to play an important role in magnetic dynamics.

Implications

Our results have important consequences for interpreting many types of experiments on spin torque. Up to now, it has been assumed almost universally in analysing experimental data that the bias dependence of the spin-torque vector can be described by the simplest possible low-order Taylor series approximations, $\tau_{\parallel} \propto V$ and $\tau_{\perp} = a + bV + cV^2$, with a, b, and c constants. This is often done, for example in extrapolating from finite-temperature measurements to determine zero-temperature critical currents and activation energy barriers for switching[29–32], and it is also the underlying assumption in analysing the statistics of switching to determine the strength of the spin-torque vector[10,11]. Our measurements indicate that these Taylor-series approximations can become seriously inaccurate at high bias, so that extrapolations based on these approximations should not be expected to yield quantitative results. Furthermore, analyses of asymmetric MTJs have generally assumed that the main effect of the asymmetry on the perpendicular torque is to add a linear bias dependence to $\tau_{\perp}(V)$, together with the quadratic dependence present for symmetric junctions[11]. The difference in the saturated values of $\partial\tau_{\perp}/\partial V$ for positive and negative V that we observe at high bias indicates that the effects of asymmetry may be significantly larger at high bias than at low bias, and may take functional forms different from those that can be expressed by a lowest-order Taylor approximation.

The asymmetry we observe for the in-plane spin torque may help to explain the observation that the critical voltage for spin-torque-induced switching from the antiparallel (AP) to parallel (P) configuration in MTJs (negative bias in our convention) is often lower than for P-to-AP switching[8,11,33–36]. However, we note that in the thermally assisted switching regime this effect can be somewhat mitigated by a contribution from the perpendicular spin torque, which always favours the AP state for our MTJs.

Applied more broadly, we expect that our time-resolved measurement technique will also be able to provide new insights about a wide range of other interesting phenomena in MTJs, including nonlinear magnetic dynamics in response to large spin torques[37], phase locking of magnetic auto-oscillations to microwave inputs[38,39], time-resolved coupling between magnetic modes, and spin torques in very low-*RA* MTJs for which pinholes may contribute new effects[12,20].

Methods

The microwave (RF) pulse in our measurement is generated by using a mixer and a short gating pulse to modulate a continuous-wave source. The peak-to-peak voltage produced by the RF pulse at the MTJ is 20–40 mV, the pulse length is 5–10 ns, and the rise and fall times of the RF pulse are approximately 100 ps and 180 ps respectively. The small non-zero fall time has negligible effect on determining the amplitude and phase of the damped precession after the pulse because (by defining the centre of the fall time as time zero) the extra torque after time zero and the reduced torque before time zero cancel to first order. There is some ringing following the RF pulse, but its amplitude is at least a factor of 25 smaller than the main excitation signal and our calculations indicate that spin torque from the ringing also has negligible effect on our final results.

The RF pulse is combined with the longer (25 ns) square-wave pulse via a power combiner. Employing a square-wave pulse instead of an actual d.c. voltage to bias the MTJ significantly reduces the probability of electrical breakdown at high voltages and allows us to access higher biases than in d.c.-detected ST-FMR or TE-FMR experiments. A sinusoidal reference signal generated by the RF source is used to synchronize the clock of the oscilloscope and is also used (after frequency division) to trigger both pulse generators and the oscilloscope at 100 kHz. These synchronization measures fix the phase of the RF pulse and allow for signal averaging. We generally average for 25 s (about 1,250 repetitions for 2,000 sampling points).

Calibration procedures and the methods used to measure the differential resistance R_0 and the d.c. resistance R at high biases are described in Supplementary Note S5.

We characterize the device capacitance by measuring the phase shift of a reflected microwave pulse before and after the microwave probe touches the sample contacts (for applied magnetic fields such that no magnetic dynamics are excited). A capacitance should produce an extra absolute phase delay $2(50\,\Omega)\omega C$. We measure a phase delay of at most 0.15 rad at 5 GHz, which corresponds to $C \leq 5 \times 10^{-14}$ F. In the ST-FMR measurement with time-domain detection, C produces an extra *relative* phase delay between the magnetic response signal and the reflected drive voltage of $\Delta\Phi = (50\,\Omega/R_0)2(50\,\Omega)\omega C$. For typical sample parameters $R_0 = 350\,\Omega$ and $\omega = 2\pi(5\,\text{GHz})$, this extra phase is less than 0.03 rad, smaller than our fitting uncertainty.

Received 1 October 2010; accepted 17 January 2011; published online 27 February 2011

References

1. Slonczewski, J. C. Current-driven excitation of magnetic multilayers. *J. Magn. Magn. Mater.* **159,** L1–L7 (1996).
2. Berger, L. Emission of spin waves by a magnetic multilayer traversed by a current. *Phys. Rev. B* **54,** 9353–9358 (1996).
3. Ralph, D. C. & Stiles, M. D. Spin transfer torques. *J. Magn. Magn. Mater.* **320,** 1190–1216 (2008).
4. Katine, J. A. & Fullerton, E. E. Device implications of spin-transfer torques. *J. Magn. Magn. Mater.* **320,** 1217–1226 (2008).
5. Tulapurkar, A. A. *et al.* Spin-torque diode effect in magnetic tunnel junctions. *Nature* **438,** 339–342 (2005).
6. Sankey, J. C. *et al.* Spin-transfer-driven ferromagnetic resonance of individual nanomagnets. *Phys. Rev. Lett.* **96,** 227601 (2006).
7. Sankey, J. C. *et al.* Measurement of the spin-transfer-torque vector in magnetic tunnel junctions. *Nature Phys.* **4,** 67–71 (2008).
8. Kubota, H. *et al.* Quantitative measurement of voltage dependence of spin-transfer torque in MgO-based magnetic tunnel junctions. *Nature Phys.* **4,** 37–41 (2008).
9. Wang, C. *et al.* Bias and angular dependence of spin-transfer torque in magnetic tunnel junctions. *Phys. Rev. B* **79,** 224416 (2009).
10. Li, Z. *et al.* Perpendicular spin torques in magnetic tunnel junctions. *Phys. Rev. Lett.* **100,** 246602 (2008).
11. Oh, S-C. *et al.* Bias-voltage dependence of perpendicular spin-transfer torque in asymmetric MgO-based magnetic tunnel junctions. *Nature Phys.* **5,** 898–902 (2009).
12. Devolder, T. *et al.* Direct measurement of current-induced fieldlike torque in magnetic tunnel junctions. *J. Appl. Phys.* **105,** 113924 (2009).
13. Petit, S. *et al.* Spin-torque influence on the high-frequency magnetization fluctuations in magnetic tunnel junctions. *Phys. Rev. Lett.* **98,** 077203 (2007).
14. Petit, S. *et al.* Influence of spin-transfer torque on thermally activated ferromagnetic resonance excitations in magnetic tunnel junctions. *Phys. Rev. B* **78,** 184420 (2008).
15. Deac, A. M. *et al.* Bias-driven high-power microwave emission from MgO-based tunnel magnetoresistance devices. *Nature Phys.* **4,** 803–809 (2008).
16. Jung, M. H., Park, S., You, C-Y. & Yuasa, S. Bias-dependences of in-plane and out-of-plane spin-transfer torques in symmetric MgO-based magnetic tunnel junctions. *Phys. Rev. B* **81,** 134419 (2010).
17. Heinonen, O. G., Stokes, S. W. & Yiet, J. Y. Perpendicular spin torque in magnetic tunnel junctions. *Phys. Rev. Lett.* **105,** 066602 (2010).
18. Polianski, M. L. & Brouwer, P. W. Current-induced transverse spin-wave instability in a thin nanomagnet. *Phys. Rev. Lett.* **92,** 026602 (2004).
19. Stiles, M. D., Xiao, J. & Zangwill, A. Phenomenological theory of current-induced magnetization precession. *Phys. Rev. B* **69,** 054408 (2004).
20. Houssameddine, D. *et al.* Spin transfer induced coherent microwave emission with large power from nanoscale MgO tunnel junctions. *Appl. Phys. Lett.* **93,** 022505 (2008).
21. Slonczewski, J. C. & Sun, J. Z. Theory of voltage-driven current and torque in magnetic tunnel junctions. *J. Magn. Magn. Mater.* **310,** 169–175 (2007).
22. Kittel, C. *Introduction to Solid State Physics* 7th edn, 505 (John Wiley, 1996).
23. Slonczewski, J. C. Currents, torques, and polarization factors in magnetic tunnel junctions. *Phys. Rev. B* **71,** 024411 (2005).
24. Theodonis, I., Kioussis, N., Kalitsov, A., Chshiev, M. & Butler, W. H. Anomalous bias dependence of spin torque in magnetic tunnel junctions. *Phys. Rev. Lett.* **97,** 237205 (2006).
25. Wilczynski, M., Barnas, J. & Swirkowiz, R. Free-electron model of current-induced spin-transfer torque in magnetic tunnel junctions. *Phys. Rev. B* **77,** 054434 (2008).
26. Xiao, J., Bauer, G. E. W. & Brataas, A. Spin-transfer torque in magnetic tunnel junctions: scattering theory. *Phys. Rev. B* **77,** 224419 (2008).
27. Manchon, A., Zhang, S. & Lee, K-J. Signatures of asymmetric and inelastic tunneling on the spin torque bias dependence. *Phys. Rev. B* **82,** 174420 (2008).
28. Heiliger, C. & Stiles, M. D. *Ab initio* studies of the spin-transfer torque in magnetic tunnel junctions. *Phys. Rev. Lett.* **100,** 186805 (2008).
29. Li, Z. & Zhang, S. Thermally assisted magnetization reversal in the presence of a spin-transfer torque. *Phys. Rev. B* **69,** 134416 (2004).
30. Fuchs, G. D. *et al.* Adjustable spin torque in magnetic tunnel junctions with two fixed layers. *Appl. Phys. Lett.* **86,** 152509 (2005).
31. Diao, Z. *et al.* Spin transfer switching and spin polarization in magnetic tunnel junctions with MgO and AlO_x barriers. *Appl. Phys. Lett.* **87,** 232502 (2005).
32. Ikeda, S. *et al.* Magnetic tunnel junctions for spintronic memories and beyond. *IEEE Trans. Electron Devices* **54,** 991–1002 (2007).
33. Yoshikawa, M. *et al.* Estimation of spin transfer torque effect and thermal activation effect on magnetization reversal in CoFeB/MgO/CoFeB magnetoresistive tunneling junctions. *J. Appl. Phys.* **101,** 09A511 (2007).
34. Devolder, T. *et al.* Single-shot time-resolved measurement of nanosecond-scale spin-transfer induced switching: stochastic versus deterministic aspects. *Phys. Rev. Lett.* **100,** 057206 (2008).
35. Lee, K. & Kang, S. H. Design consideration of magnetic tunnel junctions for reliable high-temperature operation of STT-MRAM. *IEEE Trans. Magn.* **46,** 1537–1540 (2010).
36. Chen, E. *et al.* Advances and future prospects of spin-transfer torque random access memory. *IEEE Trans. Magn.* **46,** 1873–1878 (2010).
37. Chen, W., de Loubens, G., Beaujour, J-M. L., Sun, J. Z. & Kent, A. D. Spin-torque driven ferromagnetic resonance in a nonlinear regime. *Appl. Phys. Lett.* **95,** 172513 (2009).
38. Rippard, W. H. *et al.* Injection locking and phase control of spin transfer nano-oscillators. *Phys. Rev. Lett.* **95,** 067203 (2005).
39. Grollier, J., Cros, V. & Fert, A. Synchronization of spin-transfer oscillators driven by stimulated microwave currents. *Phys. Rev. B* **73,** 060409 (2006).

Acknowledgements

We thank D. Mauri of Hitachi Global Storage Technologies (now at Western Digital Corp.) for providing the junction thin film stacks that we used to fabricate the tunnel junctions. Cornell acknowledges support from ARO, ONR, DARPA, NSF (DMR-1010768), and the NSF/NSEC program through the Cornell Center for Nanoscale Systems. We also acknowledge NSF support through use of the Cornell Nanofabrication Facility/NNIN and the Cornell Center for Materials Research facilities.

Author contributions

C.W. played the primary role in designing and performing the experiment and analysing the data. J.A.K. led the sample fabrication. Y-T.C. assisted in the measurements. All of the authors contributed to the data analysis and the preparation of the manuscript.

Additional information

The authors declare no competing financial interests. Supplementary information accompanies this paper on www.nature.com/naturephysics. Reprints and permissions information is available online at http://npg.nature.com/reprintsandpermissions. Correspondence and requests for materials should be addressed to D.C.R.